Phillips, O. M. (1985). " Spectral and statistical properties of the equilibrium range in wind-generated gravity waves." J.Fluid Mech., 156, 505=531.

Tayfun, M. A. (1986). " On narrow-band representation of ocean waves." J. Geophys. Res., 91(C6), 7743-7759.

Tayfun, M. A., and Lo, J-M. (1990). " Nonlinear effects on wave envelope and phase." J. Wtrwy., Port, Coast., and Oc. Engrg., ASCE, 116(1), 79-100.

Tayfun, M. A. (1990). " High-wave-number/frequency attenuation of wind-wave spectra." J. Wtrwy., Port, Coast., and Oc. Engrg., ASCE, 116(3), 381-398.

MODELING BOTTOM FRICTION IN WIND-WAVE MODELS [1]

Hendrik L. Tolman [2]

ABSTRACT

Effects of bottom friction in wind-wave models are investigated, with an emphasis on wave-induced bottom roughnesses (moveable-bed effects). A state-of-the-art bottom friction model is defined, based on literature. An analysis of this model indicates that, initial ripple-formation is important for swell propagation, but that moveable-bed effects are less important for depth-limited wind-seas. The small spatial decay scales associated with swell call for a sub-grid approach in (large-scale) numerical models. A sub-grid model is developed and applied successfully to swell and wind-sea cases, removing (unrealistically) large effects of sediment parameters in the later cases. Finally, implications for wave observations and sediment transport are discussed briefly.

1 Introduction

Wind-waves in oceans and shelf seas are generally described with their surface elevation ("energy") spectra, the development of which is described using a spectral balance equation. In shallow water wave-bottom interactions become a potentially important source term in the wave energy balance. An early review of such source terms is given by Shemdin et al. (1978), who consider percolation, bottom motion, bottom-friction and scattering of wave energy. For sandy bottoms, as found in many shelf seas, Shemdin et al. (1978) expect

[1] OPC Contribution No.76.

[2] UCAR visiting scientist, Marine Prediction Branch, Development Division, NOAA/NMC21, 5200 Auth Road Room 206, Camp Springs, MD 20746, USA.

bottom-friction to be dominant, in particular when the near-bottom wave motion is sufficiently strong to generate sediment transport and corresponding bed-forms (ripple-formation). In fact, only ripple-formation can explain the large range of friction factors observed for swell in nature [Shemdin et al. (1978)], and the large friction factors for laboratory experiments with irregular waves [Madsen and Rosengaus (1988), Madsen et al. (1990)]. However, in modeling bottom friction in numerical wind-wave models, the attention is usually focussed on hydrodynamic aspects of the source term, assuming that the physical bottom roughness is known [e.g., Cavaleri and Lionello (1990), Weber (1991a,b)]. To the knowledge of the present author, efforts to explicitly model moveable-bed bottom roughnesses are presented by Graber and Madsen (1988) and Tolman (1989) only.

The present study seeks to investigate bottom friction in wind-wave models with an emphasis on moveable-bed effects. To this end, a state-of the art model is defined in section 2. In section 3, this model is analyzed with respect to occurrence of roughness regimes and space scales of decay for bottom friction. It is show that typical swell can be associated to both smooth beds and wave-induced sand ripples, and that depth-limited wind-seas are generally associated with washed-out ripples and sheet-flow roughness. It is shown, that initial ripple-formation might result in preferred wave heights for swell propagation in shelf seas away from the coast, when bottom slopes are small. The corresponding decay scales [O(10 km)], call for a sub-grid approach in numerical models. A sub-grid model is briefly described in section 4, and applied successfully to swell propagation and depth-limited wind-seas in section 5. The wind-sea cases furthermore indicate, that a sub-grid approach is essential to avoid unrealistically strong dependencies of depth-limited wave heights on sediment parameters. Finally, the present results and implications for wave observations and sediment transport studies are discussed briefly in section 6. Note that the presentation and discussion of results has to be cursory due to space limitations. The results of this study will be presented in full elsewhere.

2 A local bottom friction model

In the present study, the hydrodynamic bottom friction source term of Madsen et al. (1988) is used. This model is selected because (i) it is a simple model, yet it explicitly depends on the Nikuradse equivalent sand grain roughness k_N and (ii) for consistency with the roughness model below. This model relates the source term S_l to the surface elevation spectrum F using a drag-law approach (the subscript l denoting "local" for later comparison with a sub-grid model)

$$S_l = -f_w u_r \frac{\omega^2}{2g\sinh^2 kd} F , \tag{1}$$

$$f_w = \frac{0.08}{\mathrm{Ker}^2\left(2\sqrt{\zeta_0}\right) + \mathrm{Kei}^2\left(2\sqrt{\zeta_0}\right)} , \tag{2}$$

$$\zeta_0 = \frac{1}{21.2\kappa\sqrt{f_w}} \frac{k_N}{a_r} , \tag{3}$$

$$u_r = \left\{\int \frac{2\omega^2}{\sinh^2 kd} F\right\}^{\frac{1}{2}} , \quad a_r = \left\{\int \frac{2}{\sinh^2 kd} F\right\}^{\frac{1}{2}} , \tag{4}$$

where $\omega = 2\pi f$ is the radian frequency, d is the depth, f_w is the wave friction factor, κ is the Von Kàrmàn constant, Ker and Kei are Kelvin functions of the zeroth order and u_r and a_r are the representative near-bottom orbital velocity and amplitude, obtained by integration over F. Note that f_w is a function of k_N/a_r only, and that f_w is constant for $k_N/a_r > 1$ ($f_w = 0.236$ in the present model). Note furthermore, that this model shows a relation between the roughness k_N and Weber's "dissipation coefficient" $C \equiv f_w u_r$ similar to that of the most advanced eddy viscosity models of Weber (1991a), the main differences being a moderate intra-spectral variation of C which is neglected here and a systematic difference between friction factors for identical roughnesses k_N, which could be interpreted as a different definition of the bottom roughness (figures not presented here).

Grant and Madsen (1982, henceforth denoted as GM) developed a semi-empirical moveable-bed roughness model based on observations for monochromatic waves. This model relates k_N to the Shields number ψ, which is defined here as [Cf. Madsen et al. (1990)]

$$\psi = \frac{f'_w u_r^2}{2(s-1)gD} , \tag{5}$$

where s is the relative density of the sediment compared to water (2.65 for quartz sands), D is a representative grain diameter and the prime indicates that the friction factor is based on skin friction, i.e., using $k_N = D$ in Eq. (3). The

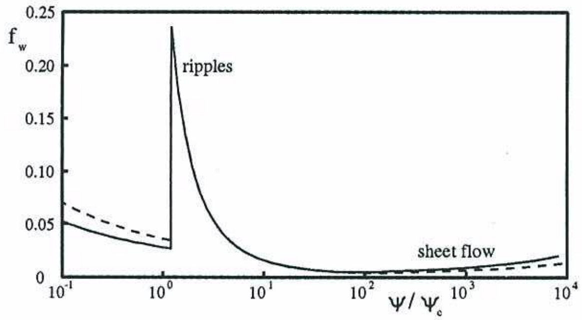

Fig. 1 Friction factors f_w as a function of the normalized Shields number ψ/ψ_c for grain diameters D = 0.1 mm (dashed line) and D = 0.4 mm (solid line) for T = 10 s, ψ_c = 0.05 (clean sand) and $k_{N,0}$ = 0.01 m.

critical Shields number for initial sediment motion ψ_c is estimated as $\psi_c \approx 0.04 \sim 0.06$ for clean, well-sorted sands [e.g., Madsen and Grant (1976), Glenn and Grant (1987)], but can become larger than 0.2 for bioturbated or multimodal sands [e.g., Drake and Cacchione (1986), Cacchione et al. (1987), Gross et al., (1992)]. If no sediment motion occurs ($\psi < \psi_c$), the bottom is assumed to be smooth [Graber and Madsen (1988) assume $k_N = D$], otherwise the roughness is comprised of ripple-roughness and sheet-flow roughness (equations not reproduced here). However, this implementation of the GM model does not seem realistic for practical conditions, because: (i) Ripples are generally much smoother for irregular waves than for monochromatic waves [e.g., Dingler and Inman (1976), Nielsen (1981), Madsen et al. (1990), Ribberink and Al-Salem (1990)]. (ii) The sheet-flow roughness term appears to over-estimate more recent data by an order of magnitude [e.g., Wiberg and Rubin (1989)]. (iii) Roughnesses for conditions without wave-induced sediment motion are typically much larger than the representative grain diameter due to bioturbation, current-induced ripples and relict bed forms [e.g., Amos et al. (1988)]. The present study therefore uses a roughness formulation similar to the GM model, but based on more recent studies, with for $\psi > 1.2\psi_c$

$$\frac{k_N}{a_r} = 1.5\left(\frac{\psi}{\psi_c}\right)^{-2.5} + 0.0655\left(\frac{u_r^2}{(s-1)g a_r}\right)^{1.4} . \qquad (6)$$

The first term represents ripple-roughness [Madsen et al. (1990)] and the

second term represents sheet-flow roughness [based on Wilson (1989), derivation not presented here]. For $\psi < 1.2\psi_c$ a constant "base roughness" $k_{N,0} >> D$ is assumed, which is typically 0.01 m. The behavior of the present ripple-roughness model is illustrated in Fig. 1. If near-bottom wave-motion is too weak to generate sediment transport ($\psi/\psi_c < 1.2$), the base-roughness $k_{N,0}$ generally results in friction factors O(0.02). At conditions of initial ripple-formation ($\psi/\psi_c \approx 1.2$) steep, well developed ripples are formed, resulting in a large relative roughness ($k_N/a_r \approx 1$) and corresponding large friction factors $f_w \approx 0.2$. For more severe near-bottom wave-motion, ripples are washed-out rapidly, so that large ripple-induced friction factors occur in a narrow range of normalized Shields numbers only. At even higher Shields number sheet-flow becomes important, and the friction factors become fairly insensitive to ψ/ψ_c.

3 Analysis of the local model

To analyze the effects of bottom friction in general and moveable beds in particular, the occurrence of roughness regimes is investigated. To promote insight, wave conditions are expressed in terms of mean wave parameters such as the significant wave height H_s (= $4\sqrt{E}$, $E = \int F$), and the wavenumber and frequency corresponding to the spectral peak (k_p and f_p). In terms of these parameters, Eqs. (4) and (5) become

$$a_r = \frac{\alpha_a H_s}{2^{3/2}} \frac{1}{\sinh k_p d} \quad , \quad u_r = \frac{\alpha_u H_s}{2}\left(\frac{g}{d}\frac{k_p d}{\sinh 2k_p d}\right)^{1/2} , \qquad (7)$$

$$\psi = \frac{\alpha_u^2}{8(s-1)} \frac{H_s^2}{dD} f_w \frac{k_p d}{\sinh 2k_p d} , \qquad (8)$$

where α_a and α_u are shape factors. For near-monochromatic swells $\alpha_a \equiv \alpha_u \equiv 1$ and for typical TMA spectra [Bouws et al (1985)] $0.7 < \alpha_a , \alpha_u < 1$ (figures not presented here). Using (8), it is easily shown that typical swell conditions result in both smooth beds without sediment motion, and in rough beds related to initial ripple formation. Swells can result in significant sheet-flow roughnesses in the surf zone only. Similarly, wind-seas (described using a TMA spectrum with given steepness $k_p H_s$) can be accompanied by roughnesses ranging from smooth beds, to conditions with significant sheet-flow roughnesses (figures not presented here).

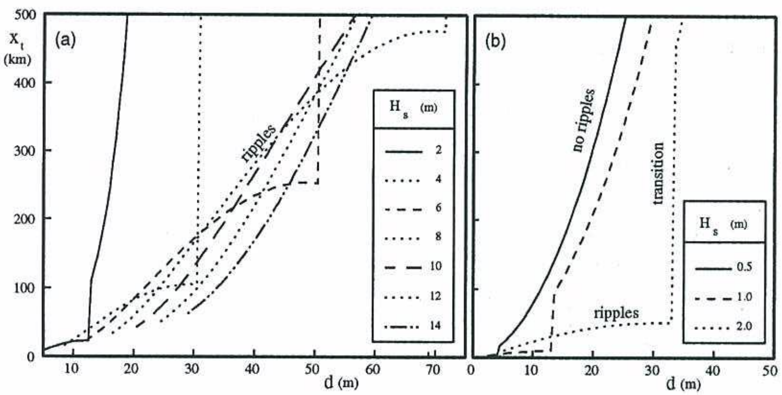

Fig. 2 Decay scales x_t for wind-seas (panel a, TMA spectra with $\gamma = 3.3$, $E = \frac{1}{4}\alpha k_p^{-2}$ and $\alpha = 0.015$) and swell (panel b, $f_p^{-1} = 12$ s). Wave heights as shown, $\psi_c = 0.05$, $D = 0.3$ mm, $k_{N,0} = 0.01$ m.

Although the occurrence of roughness regimes is interesting, it does not identify the importance of bottom friction (or ripple generation) in the overall energy balance of the wave field. This importance can be assessed without a full analysis of all source terms by analyzing decay scales related to bottom friction. An overall time scale for decay t_d can be estimated from Eq. (1) as $t_d \equiv E/\int S_1$. The corresponding spatial decay scale x_d is defined using the group velocity for the spectral peak frequency $c_{g,p}$ as $x_d \equiv c_{g,p} t_d$. After some straightforward algebraic manipulations, this decay scale becomes

$$x_d = \frac{2\sqrt{2}}{\alpha_u^3} \frac{d^2}{f_w H_s} G(k_p d) \quad , \quad G(z) = \frac{\sinh z}{z}\left[1 + \frac{\sinh 2z}{2z}\right] \quad . \tag{9}$$

In Fig. 2 decay scales x_d are presented for several wind-sea cases [panel a, TMA spectra, Bouws et al. (1985)] and several swell cases (panel b, semi-monochromatic, $f_p^{-1} = 12$ s). The sediment parameters ($k_{N,0} = 0.01$ m, $D = 0.3$ mm and $\psi_c = 0.05$) represent fairly fine, clean sand.

Fig. 2a indicates, that decay scales for wind-seas related to smooth beds are typically O(10^3 km), except for low wave heights in extremely shallow water. Such scales are generally much larger than bathymetric scales for the corresponding depths, making smooth-bed bottom friction irrelevant in the overall energy balance for wind-seas. Within the ripple regime, decay scales are

O(10^2 km), which is generally relevant in shelf seas. Severely depth-limited wind-seas are expected to generate conditions with normalized Shields numbers O(10) (figures not presented here). In such conditions, the friction factor is not very sensitive to the Shields number (see Fig. 1). Hence the friction factors and depth-limited wave heights for wind-seas are not expected to be sensitive to sediment parameters through moveable bed effects.

Fig. 2b indicates, that both smooth and rippled bottoms result in relevantly small decay scales for swell [O(100 km) and O(10 km), respectively]. As both roughness regimes are potentially important for swell propagation, the discontinuous behavior of the roughness model needs to be discussed. The roughness model (6) implies that the bottom roughness adjusts instantaneously to the wave conditions, i.e., that the time scales of ripple-adjustment are smaller that the time scales of evolution of the wave field. Within the ripple-regime, this appears to be reasonable, in conditions of initial ripple-formation (i.e., near the discontinuity of the model), it is not. In such conditions, slowly intensifying wave conditions will eventually result in initial sediment motion. This results in a rapid increase of roughness and hence in a moderation of wave conditions. Ripple build-up will stop as soon as conditions of initial sediment motion are no longer met, *regardless of the actual ripple-roughness*. Hence, ripple-roughness is partially determined by the spatial energy balance, and not solely by the local wave conditions. The corresponding wave height is the critical wave height for initial sediment motion H_c, which follows from Eq. (8) by substituting $\psi = 1.2\psi_c$

$$\frac{H_c^2}{dD} = 8(s-1)\frac{1.2\psi_c}{\alpha_u^2 f_w}\frac{\sinh 2k_p d}{k_p d} \tag{10}$$

If the bathymetric scales are larger than the decay scales corresponding to full ripple development, , this critical wave height becomes a practical maximum swell height. This is illustrated in Fig. 3, which shows swell height calculated with the following simple one-dimensional propagation model for the swell energy E.

$$\frac{\partial c_g E}{\partial x} = \int_{\text{spectrum}} S_1 \; , \tag{11}$$

where the right hand side is checked and corrected for the above mechanism of roughness generation in the regime of initial ripple-formation (details not presented here).

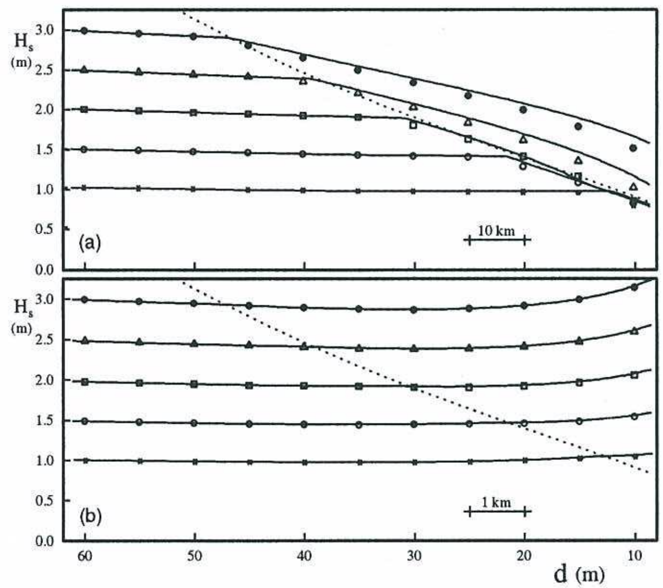

Fig. 3 One-dimensional swell propagation over a bottom with a constant slope for a "small" slope ($5\ 10^{-4}$, panel a) and a "large" slope ($5\ 10^{-3}$, panel b). Exact solution (solid lines), sub-grid numerical model (symbols) and the critical wave height for initial sediment motion H_c (dotted line). Sediment as in Fig. 2.

The solid lines in Fig. 3 represent results of this model (swell propagation form deep to shallow water) and the dotted line represents the critical wave height H_c of Eq. (10). Sediment conditions and the bottom slope are assumed constant. Note that H_c decreases monotonically with d, but not as a function of $d^{1/2}$, because f_w' implicitly varies with both H and $k_p d$.

For bottoms with a small slope (Fig. 3a) and lower input wave heights ($H_{s,d=60\ m} < 2$ m), the swell height closely follows the critical wave height, once this wave height is reached. For larger input wave heights, the reaching of the critical wave height results in a noticeable increase in wave energy dissipation, but the wave heights remain larger than H_c. This is explained as decay scales corresponding to well-developed ripples increase with increasing wave height (Fig. 2b). Apparently, the decay scale at the location where the wave height reaches H_c exceeds bathymetic scales for $H_{s,d=60\ m} > 2$ m. For much smaller bathymetric scales (i.e., larger slopes), swell heights are not noticeably influenced by H_c (Fig. 3b).

Considering the above, moveable-bed effects are potentially important, in particular for swell propagation away from the coast. Application of moveable-bed bottom friction in large-scale numerical wave models would require a sub-grid approach, because (i) the decay scale related to fully developed ripples [O(10 km)] can be significantly smaller than the grid resolution (typically 25 km or larger) and because (ii) conditions near the discontinuity in the model might not result in a roughness representative for an entire grid-box with variable sediments, depths and wave conditions. A sub-grid version of the present bottom friction source term is outlined below.

4 A sub-grid model

To account for sub-grid variations of bottom friction, an average source term representative for a grid-box has been derived, based on the local (instantaneous) application of the discontinuous roughness model (6). The derivation of a full model and the application of subsequent simplifications will be presented elsewhere. Here, only the background of the model is discussed, and the suggested source term is presented.

The roughness model (6) is a discontinuous function of the normalized Shields number $\psi_n \equiv \psi / \psi_c$. A representative (continuous) source term for a grid box is obtained by locally applying (6), using statistical properties of ψ_n and Bayes' theorem. Statistical properties of ψ_n are governed by statistical properties of d, D, ψ_c and the spectrum F [Eqs. (5) and (1) through (4)]. However, due to the integral nature of the Shields number, the two-dimensional spectrum F can be replaced by integral wave parameters H_s and f_p, assuming that the shape factors α_a and α_u are constant for the grid box. Given the law of large numbers, the pdf of ψ_n closely follows the normal distribution (as is easily confirmed using Monte Carlo simulations). Its mean value is estimated from the mean values of d, D, ψ_c, H_s and f_p and its spread σ_ψ is estimated from the corresponding spreads by linearizing (8). Using the pdf of ψ_n and Bayes' theorem, a general representative source term is obtained. After some straight-forward simplifications, the resulting model consists of the hydrodynamic model of Eqs. (1) through (4), combined with the a representative roughness $k_{N,r}$

$$\frac{k_{N,r}}{a_r} = P_I \frac{k_{N,0}}{a_r} + P_{II} \left[1.5\, \psi_{n,r}^{-2.5} + 0.0655 \left(\frac{u_r^2}{(s-1) g a_r} \right)^{1.4} \right] , \qquad (12)$$

$$\psi_{n,r} = \psi_n + p\left(\frac{1.2-\psi_n}{\sigma_\psi}\right)\frac{\sigma_\psi}{P_{II}} , \tag{13}$$

where P_I (P_{II}) represents the probability that $\psi_n < 1.2$ ($\psi_n \geq 1.2$), $\psi_{n,r}$ is the representative normalized Shields number for the ripple regime and $p(..)$ represent the standard normal pdf. P_I and P_{II} are calculated assuming a normal distribution of ψ_n. Other parameters in these equations follow directly from the (mean) depth, sediment parameters and the spectrum at the grid point. To evaluate Eqs. (12), (13) and (13), an expression for the spread σ_ψ is required. Formally, this expression depends on spreads of all five input parameters to the Shields number, as well as their correlations. For practical purposes, the following (semi-empirical) expression is suggested.

$$\frac{\sigma_\psi}{\psi_n} \approx \left[\sigma_{r,0}^2 + \left(\frac{k_p d}{\tanh k_p d} \frac{\sigma_{d,g}+\sigma_{d,s}}{d} \right)^2 \right]^{1/2} , \tag{14}$$

where $\sigma_{r,0}$ is a representative (normalized) spread, describing the combined variabilities of D, ψ_c and H_s, $\sigma_{d,g}$ represents the variability of the depth at the grid scale (which can be estimated from depths at surrounding points) and $\sigma_{d,s}$ represents an additional sub-grid variability of the depth. This particular formulation is suggested because (i) σ_ψ / ψ_n is directly related to the spread of D, ψ_c and H_s, whereas its relation to σ_d is a strong function of $k_p d$, because (ii) the latter results in systematically different behavior for swell and wind-seas and because (iii) $\sigma_{d,g}$ dominates σ_d and is easily obtained from the model grid.

5 Applications

To test the sub-grid bottom-friction source term presented in the previous section, it has been implemented in the third-generation wave model WAVEWATCH [Tolman (1989), (1991)]. For cases without currents this model solves an energy balance equation for the spectrum $F(f,\theta)$

$$\frac{\partial F(f,\theta)}{\partial t} + \nabla_x [c_g F(f,\theta)] = S(f,\theta) , \tag{15}$$

where S represents the net source term. The present version of this model uses

source terms identical to those of cycle 4 of the WAM model [WAMDI group (1988)], as described in detail by Mastenbroek et al. (1993). It furthermore includes improved numerical schemes for propagation and source term integration [Tolman (1992)]. With this model, several idealized swell and wind-sea cases have been assessed.

5.1 Swell propagation

First, the numerical model has been used to simulate the swell propagation cases presented in Fig. 3. For the small-slope case (Fig. 3a), a grid increment Δx = 10 km and a time step Δt = 6 min have been used. For the large-slope case, Δx and Δt were reduced by a factor 10. σ_ψ / ψ_n was obtained from Eq. (14), using $\sigma_{r,0} = \sigma_{d,s} = 0$, and with $\sigma_{d,g}$ calculated from the actual bottom profile. Steady results where obtained by defining a constant deep-water boundary condition, and running the model for a sufficiently long time interval.

The numerical results (symbols in Fig. 3) follow the "exact" solution (solid lines) closely, clearly identifying the different effects of initial ripple formation at the different scales. The numerical results diverge somewhat from the exact solution for the highest wave heights in the small-slope case only (solid circles and triangles in Fig. 3a). Such divergence is implicit to the moveable-bed bottom friction model for wave heights slightly larger than H_c: an overestimation of dissipation will draw the wave height closer to conditions of initial ripple formation, resulting in a (significantly) increased dissipation, drawing the wave height even closer to H_c.

5.2 Depth-limited wind-seas

Depth-limited wave heights are assessed by considering steady wave spectra for constant wind speeds, water depths and sediment parameters assuming quasi-homogeneous conditions [i.e., neglecting the second term in Eq. (15)]. Sub-grid variability of depth and sediment parameters, however, is assumed to exists. The spectrum is discretized using 24 directions ($\Delta\theta$ = 15°) and 25 frequencies, ranging from 0.04 Hz to 0.45 Hz with an increment $\Delta f = 0.1 f$ (Cf. the WAM model). The model independently determines the integration time step ($\Delta t \leq$ 15 min). Computations start from an arbitrary (small) JONSWAP spectrum, and are performed until a steady solution is reached. As an illustration, depth-limited wave heights H_d are presented as a function of the wind speed at 10 m height U_{10} in Fig. 4 for a case with d = 20 m, D = 0.2 mm, ψ_c = 0.05 (clean sand) and $k_{N,0}$ = 0.01 m. Results are presented for the discontinuous model (dashed line), the sub-grid model with $\sigma_{r,0}$ = 0.2 and $(\sigma_{d,g}+\sigma_{d,s})/d$ = 0.2 (solid

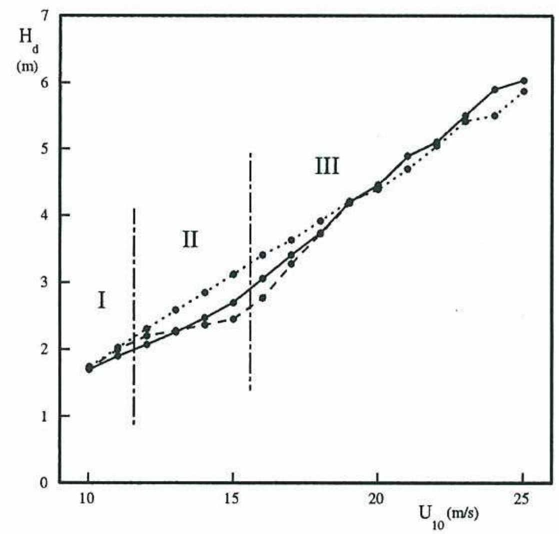

Fig. 4 Numerical simulation of depth-limited wave heights H_d for homogeneous conditions as a function of the wind speed U_{10}. The present sub-grid model (solid line, $\sigma_{r,0} = 0.2$ and $(\sigma_{d,g}+\sigma_{d,s})/d = 0.2$), the discontinuous model on which it is based (dashed line) and a constant roughness model ($k_N \equiv k_{N,0}$, dotted line). $d = 20$ m, $D = 0.2$ mm, $\psi_c = 0.05$ and $k_{N,0} = 0.01$ m. The symbols represent the actual model results.

line) and a (conventional) model with a constant roughness length $k_N = 0.01$ m (dotted line).

The results for the discontinuous model in Fig. 4 (dashed line) show clearly discontinuous behavior. For low wind speeds (range marked as I) near-bottom wave motion is insufficient to move sediment, and H_d increases with U_{10}. For a fairly broad range of intermediate wind speeds (range II in Fig. 4), conditions of initial ripple formation occur, where the actual bottom roughness is governed by the source term balance. In this range, the dependency of H_d on U_{10} is practically negligible. Note that the results in range II appear to be independent of initial conditions (figures not presented here), so that the discontinuous behaviour does not seem to generate "chaotic" behavior (bifurcations). For the higher wind speeds of region III, the wind is sufficiently strong to "break through" the discontinuity and reach the ripple regime, where H_d again increases with U_{10}. As conditions of initial ripple-formation are sensitive to sediment parameters, H_d of the discontinuous model is potentially sensitive to

sediment parameters. This is an artifact of the application of the discontinuous model to the entire grid-box, as follows from a comparison with the sub-grid model. Although the latter model (solid line) still shows some effects of the moveable bed roughness when compared to the constant roughness model (dotted lines), such effects are mild and do not show any discontinuities. Note that much smaller spreads of the Shields number than applied here are sufficient to remove the discontinuities of H_d related to the discontinuous nature of the local model.

6 Discussion and conclusions

An analysis of the decay scales related to bottom friction for a state-of-the-art moveable-bed bottom-friction model indicates that initial ripple-formation is potentially important for swell propagation over mildly sloping bottoms. In fact, the discontinuous transition between flat beds and sand ripples results in a non-local mechanism of roughness generation and energy decay. It is unlikely, that such a mechanism is described accurately by previous models, which do not explicitly consider moveable-bed effects. For depth-limited wind-seas moveable-bed effects are less important, because such wave conditions are generally accompanied by washed-out ripples, where the roughness is fairly insensitive to sediment or wave parameters.

Initial ripple-formation can results in length scales of energy decay, which are significantly smaller than the resolution of typical wind-wave models. Therefore, a sub-grid version of the above moveable-bed bottom-friction model has been developed. This model is shown to reproduce energy decay for swell propagation in conditions of initial ripple-formation, in spite of the somewhat unstable model characteristics in such conditions. Model results furthermore indicate, that a sub-grid model is essential to avoid an unrealistically strong dependency of wind-sea wave-heights on sediment parameters for mildly depth-limited conditions.

Moveable-bed effects are also expected to be important in analyzing wave observations. Roughness generation by swell in conditions of initial ripple-formation represents a clearly different dissipation mechanism than the conventional constant roughness concept. Analyzing results as presented in Fig. 3a in a conventional way by fitting a single friction factor gives results without a physical meaning. Clearly, sediment data is imperative in interpreting swell decay data. Observations of depth-limited wind-seas generally consider extremely shallow water and high wind speeds, typically corresponding to range

III in Fig. 4. In such conditions, constant roughness and moveable-bed models (dotted and solid lines, respectively) result in similar wave heights H_d, indicating that sediment parameters are not expected to have a large impact on such observations. In more mildly depth-limited conditions (range II in Fig. 4), this is not necessarily the case, making such conditions interesting for further research.

Finally, the mechanism for roughness generation in conditions of initial ripple formation has an interesting implication for sediment transport. In the Sediment transport literature, large wave-generated roughnesses are usually implied from large suspended sediment concentrations. If, however, roughnesses are related to the spatial energy balance or the source term balance, sediment transport is by definition small, but roughnesses can reach their maximum.

Acknowledgements. The present study was initiated while the author held an NRC resident research associateship at NASA / Goddard Space Flight Center, and was finished at NOAA / NMC.

REFERENCES

Amos, C.L., A.J. Bowen, D.A. Huntley and C.F.M. Lewis, 1988: Ripple generation under combined influence of waves and currents on the Canadian continental shelf. *Cont. Shelf Res.*, **8**, 1129-1153.

Bouws, E., H. Günter, W. Rosenthal and C.L. Vincent, 1985: Similarity of the wind wave spectrum in finite depth water. 1: Spectral form. *J. Geophys. Res.*, **90**, 975-986.

Cacchione, D.A. , W.D. Grant, D.E. Drake and S.M. Glenn, 1987: Storm-dominated bottom boundary layer dynamics on the northern California continental shelf: Measurements and predictions. *J. Geophys. Res.*, **92**, 1817-1827.

Cavaleri, L. and P. Lionello, 1990: Linear and non-linear approach to bottom friction in wave motion: Critical intercomparison. to *Estuarine, Coastal and Shelf Science*, **30**, 355-367.

Drake, D.E. and D.A. Cacchione, 1986: Field observations of bed shear stress and sediment resuspension on shelves. *Cont. Shelf Res.*, **6**, 415-429.

Dingler, J.R. and D.L. Inman, 1976: Wave-formed ripples in near-shore sands. *Proc. 15th Int. Conf. Coastal Eng.*, ASCE, Honolulu, 2109-2126.

Glenn, S.M. and W.D. Grant, 1987: A suspended sediment stratification correction for combined wave and current flows. *J. Geophys. Res.*, **92**, 8244-8264.

Graber, H.C., and O.S. Madsen, 1988: A finite-depth wind-wave model. Part I: Model description. *J. Phys. Oceanogr.*, **18**, 1465-1483.

Grant, W.D., and O.S. Madsen, 1982: Movable bed roughness in unsteady oscillatory flow. *J. Geophys. Res.*, **87**, 469-481.

Gross, T.F., A.E. Isley and C.R. Sherwood, 1992: Estimation of stress and bed roughness during storms on the northern California shelf. *Cont. Shelf Res.*, **12**, 389-413.

Madsen, O.S., and W.D. Grant, 1976: Quantitative description of sediment transport by waves. *Proc. 15th Int. Conf. Coastal Eng.*, ASCE, 1093-1112.

Madsen, O.S., and M.M. Rosengaus, 1988: Spectral wave attenuation by bottom friction: experiments. *Proc. 21st Int. Conf. Coastal Eng.*, ASCE, Malaga, 849-857.

——, Y.-K. Poon and H.C. Graber, 1988: Spectral wave attenuation by bottom friction: theory. *Proc. 21st Int. Conf. Coastal Eng.*, ASCE, Malaga, 492-504.

——, P.P. Mathiesen and M.M. Rosengaus, 1990: Movable bed friction factors for spectral waves. *Proc. 22st Int. Conf. Coastal Eng.*, ASCE, Delft, 420-429.

Mastenbroek, C., G. Burgers and P.A.E.M. Janssen, 1993: The dynamic coupling of a wave model and a storm surge model through the atmospheric boundary layer. *J. Phys. Oceanogr.*, in press.

Nielsen, P., 1981: Dynamics and geometry of wave-generated ripples. *J. Geophys. Res.*, **86**, 6467-6472.

Ribberink, J.S. and A. Al-Salem, 1990: Bedforms, sediment concentrations and sediment transport in simulated wave conditions. *Proc. 22nd Int. Conf. Coastal Eng.*, ASCE, Delft, 2318-2331.

Shemdin, O., K. Hasselmann, S.V. Hsiao and K. Heterich, 1978: Nonlinear and linear bottom interaction effects in shallow water, in : Turbulent fluxes through the sea surface, wave dynamics and prediction. NATO Conf. Ser. V, Vol 1, 347-365.

Tolman, H.L., 1989: The numerical model WAVEWATCH: a third generation model for the hindcasting of wind waves on tides in shelf seas. *Communications on Hydraulic and Geotechnical Engineering*, Delft Univ. of Techn., ISSN 0169-6548, Rep. No. **89-2**, 72 pp.

——, 1991: A third-generation model for wind waves on slowly varying, unsteady and inhomogeneous depths and currents. *J. Phys. Oceanogr.*, **21**, 782-797.

——, 1992: Effects of numerics on the physics in a third-generation wind-wave model. *J. Phys. Oceanogr.*, **22**, 1095-1111.

WAMDI group, 1988: The WAM model - a third generation ocean wave prediction model. *J. Phys. Oceanogr.*, **18**, 1775-1810.

Weber, S.L., 1991a: Eddy-viscosity and drag-law models for random ocean wave dissipation. *J. Fluid Mech.*, **232**, 73-98.

——, 1991b: Bottom friction for wind sea and swell in extreme depth-limited situations. *J. Phys. Oceanogr.*, **21**, 149-172.

Wiberg, P.L. and D.M. Rubin, 1989: Bed roughness produced by saltating sediment. *J. Geophys. Res.*, **94**, 5011-5016.

Wilson, K.C., 1989: Friction on wave induced sheet flow. *Coastal engineering*, **13**, 371-379.